

Small anisotropy, weak thermal fluctuations, and high field superconductivity in Co-doped iron pnictide $\text{Ba}(\text{Fe}_{1-x}\text{Co}_x)_2\text{As}_2$

A. Yamamoto, J. Jaroszynski, C. Tarantini, L. Balicas, J. Jiang, A. Gurevich,
and D.C. Larbalestier

*National High Magnetic Field Laboratory, Florida State University, Tallahassee, FL
32310, USA*

R. Jin, A.S. Sefat, M.A. McGuire, B.C. Sales, D.K. Christen, and D. Mandrus
*Materials Science & Technology Division, Oak Ridge National Laboratory, Oak Ridge,
TN 37831, USA*

We performed high-field magnetotransport and magnetization measurements on a single crystal of the 122-phase iron pnictide $\text{Ba}(\text{Fe}_{1-x}\text{Co}_x)_2\text{As}_2$. Unlike the high-temperature superconductor cuprates and 1111-phase oxypnictides, $\text{Ba}(\text{Fe}_{1-x}\text{Co}_x)_2\text{As}_2$ showed practically no broadening of the resistive transitions under magnetic fields up to 45 T. We report the temperature dependencies of the upper critical field H_{c2} both parallel and perpendicular to the c -axis, the irreversibility field $H_{\text{irr}}^c(T)$ and a rather unusual symmetric volume pinning force curve $F_p(H)$ suggestive of a strong pinning nanostructure. The anisotropy parameter $\gamma = H_{c2}^{ab}/H_{c2}^c$ deduced from the slopes of $dH_{c2}^{ab}/dT = 4.9\text{T/K}$ and $dH_{c2}^c/dT = 2.5\text{T/K}$ decreases from ~ 2 near T_c , to ~ 1.5 at lower temperatures, much smaller than γ for 1111 pnictides and high- T_c cuprates.

The discovery of superconductivity in iron oxypnictides¹ has attracted strong interest due to an unusual interplay of superconductivity and magnetism and extremely high upper critical fields H_{c2} .^{2,3} Like the high temperature superconductor (HTS) cuprates, iron pnictides are layered with alternating basal Fe-As layers sandwiched between doped charge reservoir layers. Superconductivity appears upon doping a parent antiferromagnetic state with electrons^{1,4} or holes,⁵ resulting in high transition temperatures T_c up to 55 K for the 1111 type single layer oxypnictides REFeAsO (RE = rare earth). The recently discovered 122 type AFe₂As₂ compounds (AE = alkali or alkali earth) become superconducting with T_c up to 38 K by hole doping.⁶ Electron doping induced by substituting Co⁷ or Ni⁸ for Fe can also induce superconductivity, but, unlike the cuprates, iron-pnictides can tolerate magnetic impurities in the superconducting layers.

Our previous high-field measurements on the La, Nd and Sm 1111 oxypnictides showed very high upper critical fields H_{c2} of ~ 65 T for LaFeAsO_{1-x}F_x polycrystals² and even greater than 100 T for Nd and Sm pnictides.³ However, the Nd and Sm 1111 compounds exhibit field-induced, thermally-activated broadening of the resistive transitions reminiscent of that in the cuprates. Concurrently, quasi-reversible magnetization was observed in LaFeAsO_{1-x}F_x polycrystals, indicative of weak pinning of a nearly equilibrium vortex lattice.⁹ It was also suggested that the higher- T_c oxypnictides, like the cuprates, may have a grain-boundary weak-link problem.⁹⁻¹¹ On the other hand, the 122 pnictides have lower T_c but also much lower anisotropy than the 1111 oxypnictides.¹²⁻¹⁴ Here, we report on $H_{c2}(T)$ and of the irreversibility field $H_{irr}(T)$ in Ba(Fe,Co)₂As₂ single crystals. Surprisingly, we found conventional low-temperature-superconductor-like (LTS) displacements of the resistive transition in fields up to 45 T, indications for strong vortex pinning, and a very high H_{irr} close to the onset of the superconducting transition at H_{c2} . Both H_{c2} and H_{irr} exceed the BCS paramagnetic limit at low T .

Cobalt-doped BaFe₂As₂ single crystals were synthesized by the self-flux method.⁷ The present Ba(Fe_{0.9}Co_{0.1})₂As₂ crystal has dimensions of 1.28×0.58×0.030 mm³. High-field magneto-transport measurements were performed using the National High Magnetic Field Laboratory DC 45 T hybrid magnet and a 16 T Quantum Design physical property measurement system. The full critical state magnetization was measured in an Oxford 14 T vibrating sample magnetometer.

Our crystal has T_c of 22 K inferred from the susceptibility measurements. Figure 1 shows magnetization hysteresis loops which exhibit a small “fish-tail” hump at 5-10 T, similar to that of (Ba,K)Fe₂As₂ (Ref. 15) and YBa₂Cu₃O_{7- δ} crystals.¹⁶ The critical current density J_c calculated from the width of the hysteresis loops using the Bean model is shown in Fig. 2. J_c exhibits a rapid decrease at low-fields followed by broad maxima and a relatively weak field dependence at high-fields. The self-field $J_c = 4 \times 10^5$ A/cm² at 4.2 K is indeed high for a single crystal.

To assess mechanisms, which control the vortex pinning force $F_p = \mu_0 H J_c$, we plot in Fig. 3 the normalized pinning force F_p/F_p^{\max} as a function of the reduced field $h = H/H_{irr}$. Here we define the irreversibility field H_{irr} at which $J_c(H)$ extrapolates to zero from the field closure of hysteretic magnetization loops. The normalized curves of $F_p(h, T)$ for $T > 15$ K and $(0.05-0.1) < h < 1$ collapse into a single curve described by the scaling function $h^p(1-h)^q$ with $p = 1.67$, $q = 2$ (Ref. 17). Moreover, the lower T , partial $F_p(h)$ curves taken at 4.2-12.5 K also exhibit the same field dependence, allowing H_{irr} to be estimated down to ~ 10 K. The observed F_p scaling, which is independent of temperature, suggests one dominant vortex pinning mechanism, while the symmetric $F_p(h)$ curves with a peak at $h \sim 0.45$ imply a dense vortex pinning nano-structure, perhaps due to an inhomogeneous distribution of cobalt ions, which produces a locally varying order parameter. This

scenario is consistent with a spatial variation of K in (Ba,K)Fe₂As₂ single crystals¹⁸ and similar to the field-induced pinning by oxygen deficient regions in YBa₂Cu₃O_{7- δ} .¹⁶

The results of magneto-transport measurements in fields parallel to the *c*-axis up to 45 T are shown in Fig. 4. It is clear that the $R(T)$ curves are displaced to lower temperatures upon increasing fields, but also that they do not noticeably broaden. The transition widths ΔT defined by the 90% and 10% points on $R(T)$ do not exceed 2-3 K. The transitions with fields parallel to the *ab*-plane were similarly sharp up to 45 T. This lack of broadening of the resistive transitions under field is in strong contrast to some of the 1111 oxypnictides^{2,3,19} and rather similar to a conventional LTS like Nb₃Sn.²⁰

The combined high field magneto transport and magnetization analyses enable us to obtain the magnetic phase diagram. The temperature-dependent resistive $H_{c2}(T)$ defined by 90% of R_n is shown in Fig. 5. Both H_{c2}^{ab} and H_{c2}^c exhibit almost linear temperature dependence near T_c with slopes of $dH_{c2}^{ab}/dT = 4.9$ T/K and $dH_{c2}^c/dT = 2.5$ T/K. The anisotropy $\gamma = H_{c2}^{ab}/H_{c2}^c$ varies from ~ 1.5 to 2 as T increases (see inset of Fig. 5). This temperature-dependent γ is consistent with multi-band superconductivity, however $\gamma = 1.5-2$ is significantly lower than $\gamma = 5-10$ measured on the 1111 oxypnictides.^{3,21,22} The low temperature H_{c2} extrapolates to > 60 T, much larger than the Werthamer-Helfand-Hohenberg extrapolation $H_{c2}^c(0) \sim 0.69T_c|dH_{c2}^c/dT|_{T_c} \sim 38$ T, indicating unconventional $H_{c2}(T)$ behavior. Moreover, even at $T = T_c/2$, the observed H_{c2}^{ab} already exceeds the BCS paramagnetic limit $H_p = 1.84T_c \sim 40.5$ T. Extrapolations of the $H_{c2}(T)$ data in Fig. 5 suggest $H_{c2}^{ab}(0) \sim 70$ T and $H_{c2}^c(0) \sim 50$ T, comparable to estimates of ~ 70 T for (Ba,K)Fe₂As₂¹²⁻¹⁴ and ~ 65 T for the optimally doped LaFeAsO_{0.89}F_{0.11},^{2,19} though much smaller than $H_{c2}(0) > 100$ T for Nd and Sm oxypnictides.³

Now we discuss the relationship of H_{c2} and H_{irr} defined conventionally as the field at which $J_c(H)$ extrapolates to zero, which gives $H_{irr}(T)$ close to the onset of the flux flow resistance at $R(T) = 0.1R_n$. The lack of the field-induced broadening of $R(T)$ and the fact that H_{c2} and H_{irr} are not very different indicate the LTS-like behavior, unlike HTS cuprates in which H_{irr} is well below H_{c2} due to strong thermal fluctuations of vortices. This LTS-like behavior is also consistent with weak thermal fluctuations, as follows from the estimation of the Ginzburg number²³ $Gi = (2\pi k_B T_c \mu_0 \lambda_0^2 / \Phi_0^2 \xi_c^2)^2 / 2 \sim 6.8 \times 10^{-5}$, much lower than for the least anisotropic cuprate YBa₂Cu₃O_{7- δ} ($\sim 10^{-2}$) and polycrystalline NdFeAs(O,F) and SmFeAsO_{1- δ} ($\sim 10^{-2}$) and LaFeAs(O,F) ($\sim 3.4 \times 10^{-4}$),³ and even for clean MgB₂ ($\sim 2.0 \times 10^{-4}$). Here the London penetration depths $\lambda_{ab} = 160$ nm and $\lambda_c \sim \gamma \lambda_{ab} = 320$ nm were estimated from the lower critical field $H_{c1}^{ab} \sim \Phi_0(\ln \kappa + 0.5) / 4\pi \lambda_{ab} \lambda_c$ measured from the deviation of the diamagnetic magnetization using a SQUID magnetometer, where $\kappa \sim 65$ is the Ginzburg-Landau parameter. $H_{c1}(T)$ shows the usual linear temperature dependence with $dH_{c1}^{ab}/dT = 0.79$ mT/K near T_c , extrapolating to $H_{c1}^{ab}(0) \sim 15$ mT. The coherence lengths $\xi_{ab} = 2.44$ nm and $\xi_c \sim \gamma^{-1} \xi_{ab} = 1.22$ nm were evaluated from the $H_{c2}(0)$ extrapolations.

Given the weakness of vortex thermal fluctuations, the finite width of $R(T)$ in our single crystal likely results from random T_c inhomogeneities due to local compositional variations, proximity effect near defects, etc, which cause local fluctuations of H_{c2} and the flux flow resistivity so that the curve $R(T)$ reflects the percolative transition in a weakly inhomogeneous superconductor. In this case the onset of the superconducting transition at H_{c2} represents the maximum H_{c2} . In turn, the onset of the global magnetic irreversibility at H_{irr} may be interpreted as the field percolation threshold at which the lower H_{c2} superconducting regions form an infinite percolation cluster.

In summary, our magnetization and transport measurements show very high values of H_{c2} exceeding the BCS paramagnetic limit, and lack of field-induced broadening of the

resistive transitions up to 45 T. The irreversibility field H_{irr} is close to H_{c2} , indicating weak thermal fluctuations and/or strong vortex pinning. Thus, Co-doped 122 pnictide is a quasi-LTS high field superconductor with $H_{c2} > 50$ T and weak anisotropy with $\gamma < 2$.

We are grateful to V. Griffin, N. Craig, F. Hunte, E. E. Hellstrom and M. Putti for discussions. Work at the NHMFL was supported by the NSF Cooperative Agreement DMR-0084173, by the State of Florida, by the DOE and by AFOSR under Grant No. FA9550-06-1-0474. Work at ORNL was supported by the Division of Materials Science and Engineering, Office of Basic Energy Sciences. AY is supported by a fellowship of the JSPS.

References

- ¹Y. Kamihara, T. Watanabe, M. Hirano, and H. Hosono, *J. Am. Chem. Soc.* **130**, 3296 (2008).
- ²F. Hunte, J. Jaroszynski, A. Gurevich, D. Larbalestier, R. Jin, A. Sefat, M. McGuire, B. Sales, D. Christen, and D. Mandrus, *Nature* **453**, 903 (2008).
- ³J. Jaroszynski *et al.*, *Phys. Rev. B* **78**, 064511 (2008); **78**, 174523 (2008).
- ⁴A. S. Sefat, M. A. McGuire, B. C. Sales, R. Jin, J. Y. Howe, and D. Mandrus, *Phys. Rev. B* **77**, 174503 (2008).
- ⁵H. H. Wen, G. Mu, L. Fang, H. Yang, and X. Zhu, *Europhys. Lett.* **82**, 17009 (2008).
- ⁶M. Rotter, M. Tegel, and D. Johrendt, *Phys. Rev. Lett.* **101**, 107006 (2008).
- ⁷A. S. Sefat, R. Jin, M. A. McGuire, B. C. Sales, D. J. Singh, and D. Mandrus, *Phys. Rev. Lett.* **101**, 117004 (2008).
- ⁸L. J. Li, Q. B. Wang, Y. K. Luo, H. Chen, Q. Tao, Y. K. Li, , X. Lin, M. He, Z. W. Zhu, G. H. Cao, and Z. A. Xu, *Cond-mat*, arXiv:0809.2009v1.
- ⁹A. Yamamoto, J. Jiang, C. Tarantini, N. Craig, A. Polyanskii, F. Kametani, F. Hunte, J. Jaroszynski, E. Hellstrom, D. Larbalestier, R. Jin, A. Sefat, M. McGuire, B. Sales, D. Christen, and D. Mandrus, *Appl. Phys. Lett.* **92**, 252501 (2008).
- ¹⁰R. Prozorov, M. E. Tillman, E. D. Mun, and P. C. Canfield, *Cond-mat* arXiv:0805.2783v1 (2008).
- ¹¹A. Yamamoto, A. Polyanskii, J. Jiang, F. Kametani, C. Tarantini, F. Hunte, J. Jaroszynski, E. Hellstrom, P. Lee, A. Gurevich, D. Larbalestier, Z. Ren, J. Yang, X. Dong, W. Lu, and Z. Zhao, *Supercond. Sci. Technol.* **21**, 095008 (2008).
- ¹²H. Q. Yuan, J. Singleton, F. F. Balakirev, G. F. Chen, J. L. Luo, and N. L. Wang, *Nature* **457**, 565 (2009).
- ¹³M. Altarawneh, K. Collar, C. Mielke, N. Ni, S. Bud'ko, and P. Canfield, *Phys. Rev. B* **78**, 220505 (2008).
- ¹⁴Z. S. Wang, H. Q. Luo, C. Ren, and H. H. Wen, *Phys. Rev. B* **78**, 140501(R) (2008).
- ¹⁵H. Yang, H. Luo, Z. Wang, and H. H. Wen, *Appl. Phys. Lett.* **93**, 142506 (2008).
- ¹⁶M. Daeumling, J. Seuntjens, and D. Larbalestier, *Nature* **346**, 332 (1990).
- ¹⁷E. J. Kramer, *J. Appl. Phys.* **44**, 1360 (1973).
- ¹⁸N. Ni, S. Nandi, A. Kreyssig, A. I. Goldman, E. D. Mun, S. L. Bud'ko, and P. C. Canfield, *Phys. Rev. B* **78**, 014523 (2008).
- ¹⁹Y. Kohama, Y. Kamihara, S. A. Baily, L. Civale, S. C. Riggs, F. F. Balakirev, T. Atake, M. Jaime, M. Hirano, and H. Hosono, *Cond-mat*, arXiv:0809.1133v1.
- ²⁰A. Godeke, M. Jewell, C. Fischer, A. Squitieri, P. Lee, and D. Larbalestier, *J. Appl. Phys.* **97**, 093909 (2005).
- ²¹U. Welp, R. Xie, A. E. Koshelev, W. K. Kwok, P. Cheng, L. Fang, and H. H. Wen, *Phys. Rev. B* **78**, 140510(R) (2008).
- ²²L. Balicas, A. Gurevich, Y. J. Jo, J. Jaroszynski, D. C. Larbalestier, R. H. Liu, H. Chen, X. H. Chen, N. D. Zhigadlo, S. Katrych, Z. Bukowski, and J. Karpinski, *Cond-mat*, arXiv:0809.4223v1.
- ²³G. Blatter, M. V. Feigel'man, V. B. Geshkenbein, A. I. Larkin, and V. M. Vinokur, *Rev. Mod. Phys.* **66**, 1125 (1994).

Figure captions

Fig. 1. (Color online) Magnetization hysteresis loops at 4.2, 7.5, 10, 12.5, 15, 17.5 and 20 K. Magnetic field was applied parallel to c -axis.

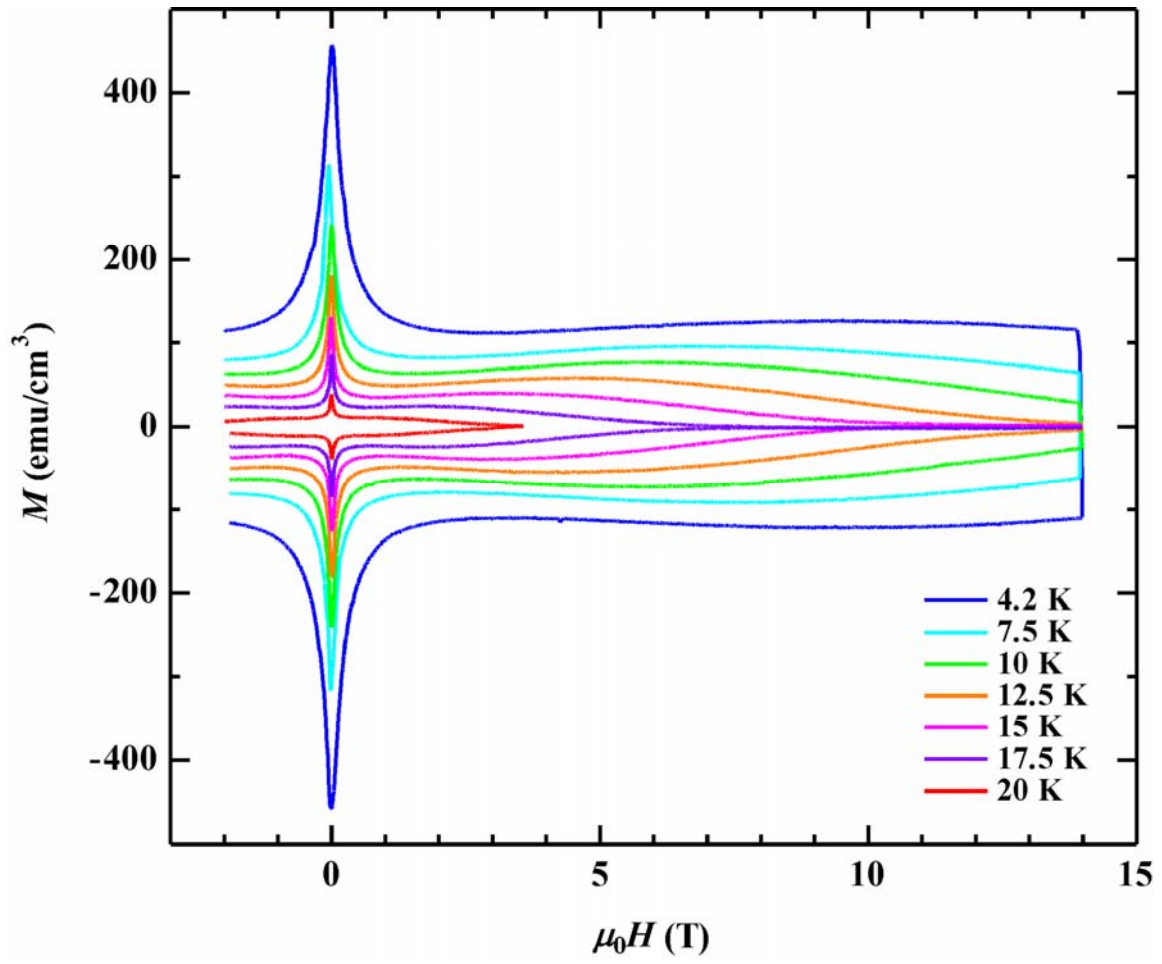
Fig. 2. (Color online) Magnetic field dependence of the in-plane critical current density J_c . Triangles indicate broad maximum positions.

Fig. 3. (Color online) Normalized flux pinning force F_p/F_p^{\max} as a function of reduced field $h = H/H_{\text{irr}}$. Dashed line represents the fitting curve $h^{1.67}(1-h)^2$. Inset shows F_p/F_p^{\max} as a function of field H .

Fig. 4. (Color online) In-plane resistivity ρ_{ab} as a function of temperatures under magnetic field of $\mu_0 H = 0, 1, 3, 6, 9, 12, 15, 20, 25, 30$ and 35 T. High field measurements above 15 T was performed using 45 T hybrid magnet at FSU.

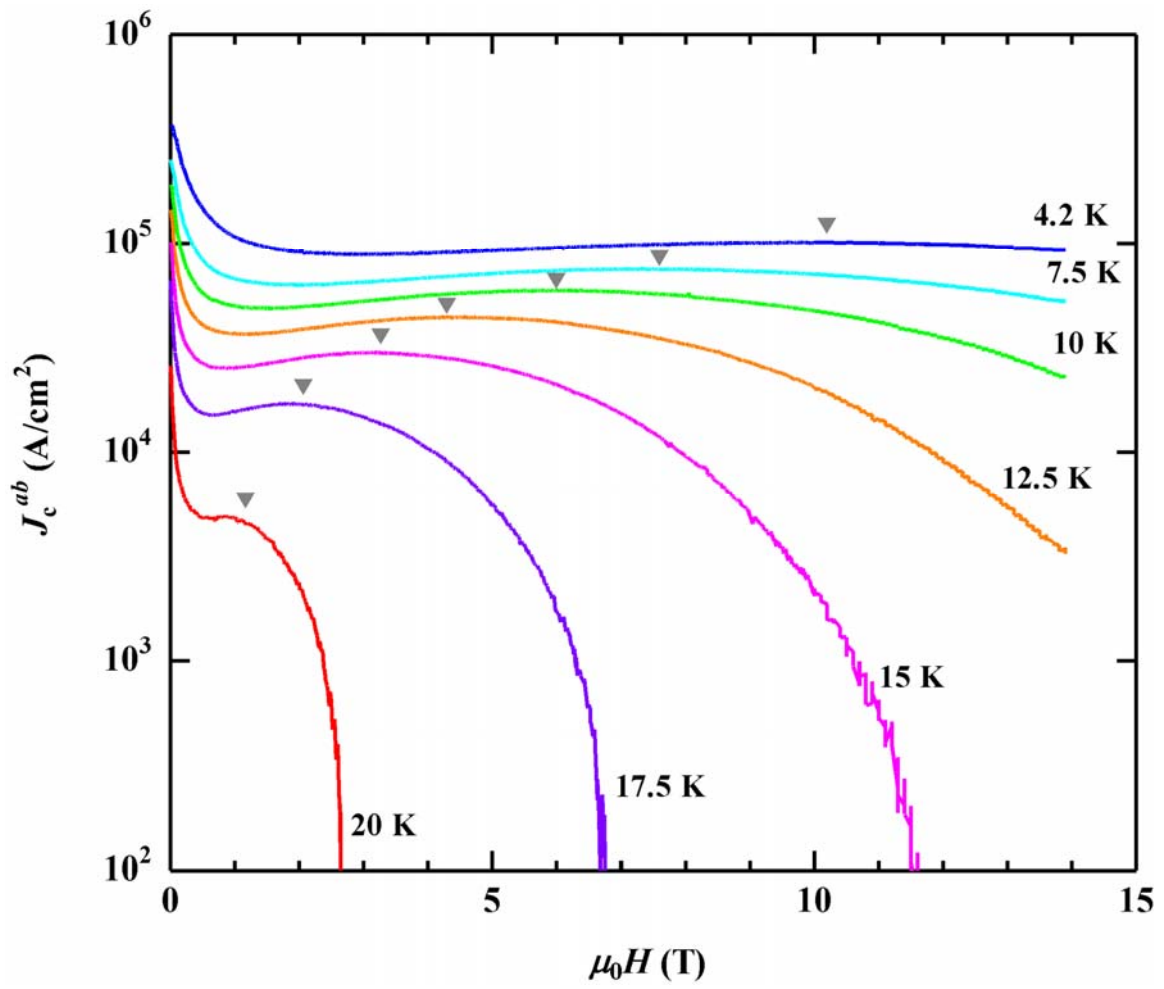
Fig. 5. (Color online) Magnetic phase diagram of the $\text{Ba}(\text{Fe}_{0.9}\text{Co}_{0.1})_2\text{As}_2$ single crystal. Filled and open symbols represent 90% and 10% of $R(T, H)$ of R_n , respectively. Circles and squares represent resistive H_{c2} parallel to the ab plane and c axis, respectively. Upward-pointing triangles represent the irreversibility field H_{irr}^c extrapolated from the pinning force curves shown in Fig. 3. For $H_{\text{irr}} > 14$ T, H_{irr} was estimated from the scaling of F_p curves as described in text. Downward-pointing triangles mark the field of fish-tail peaks on magnetic hysteresis loops. The temperature dependencies of H_{irr} and the field of the fish-tail magnetization peak can be fitted with $H^* = H^*(0) \times (1 - T/T_c)^{5/4}$. Inset shows the temperature dependence of H_{c2} anisotropy parameter $\gamma = H_{c2}^{ab}/H_{c2}^c$.

Figure 1



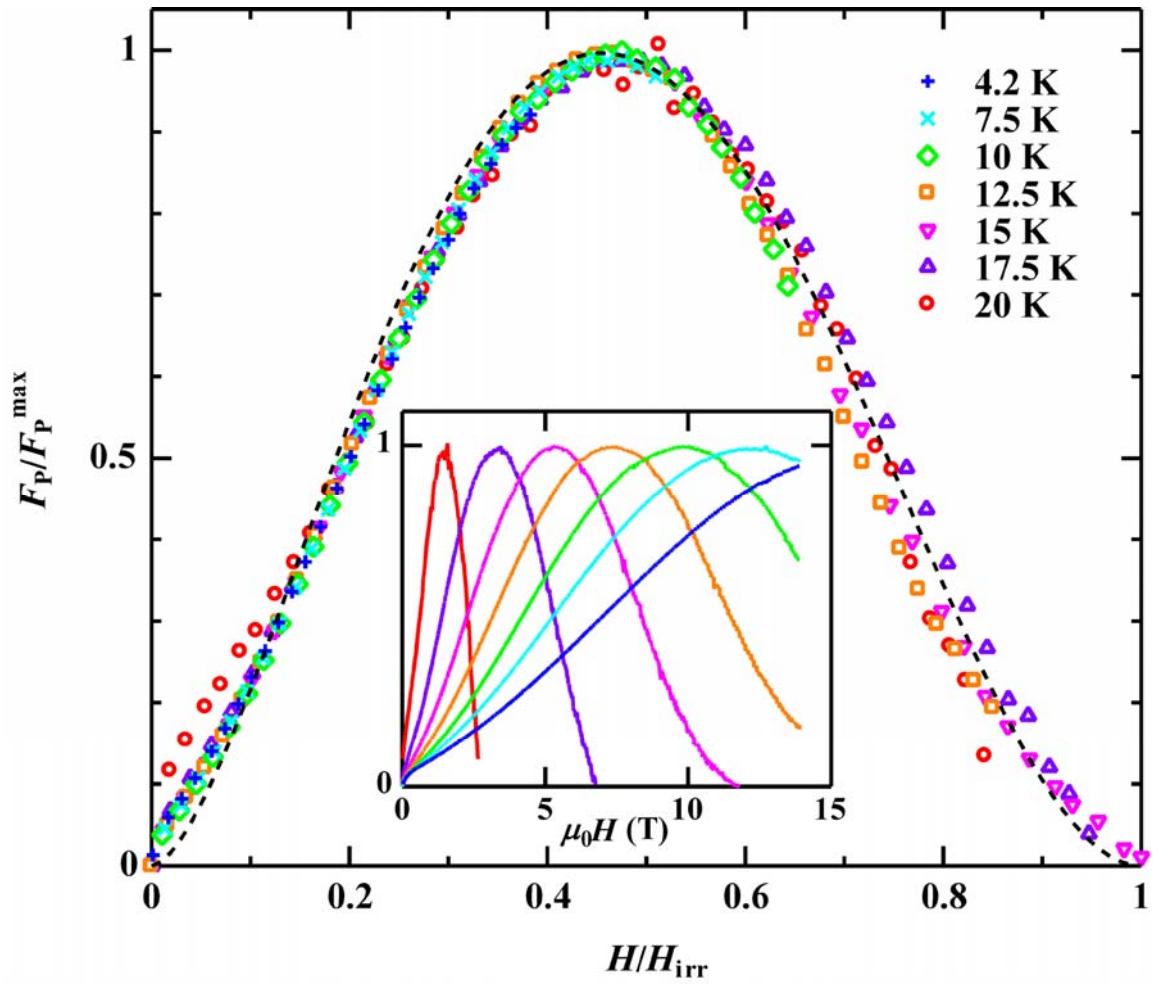
Yamamoto et al.

Figure 2



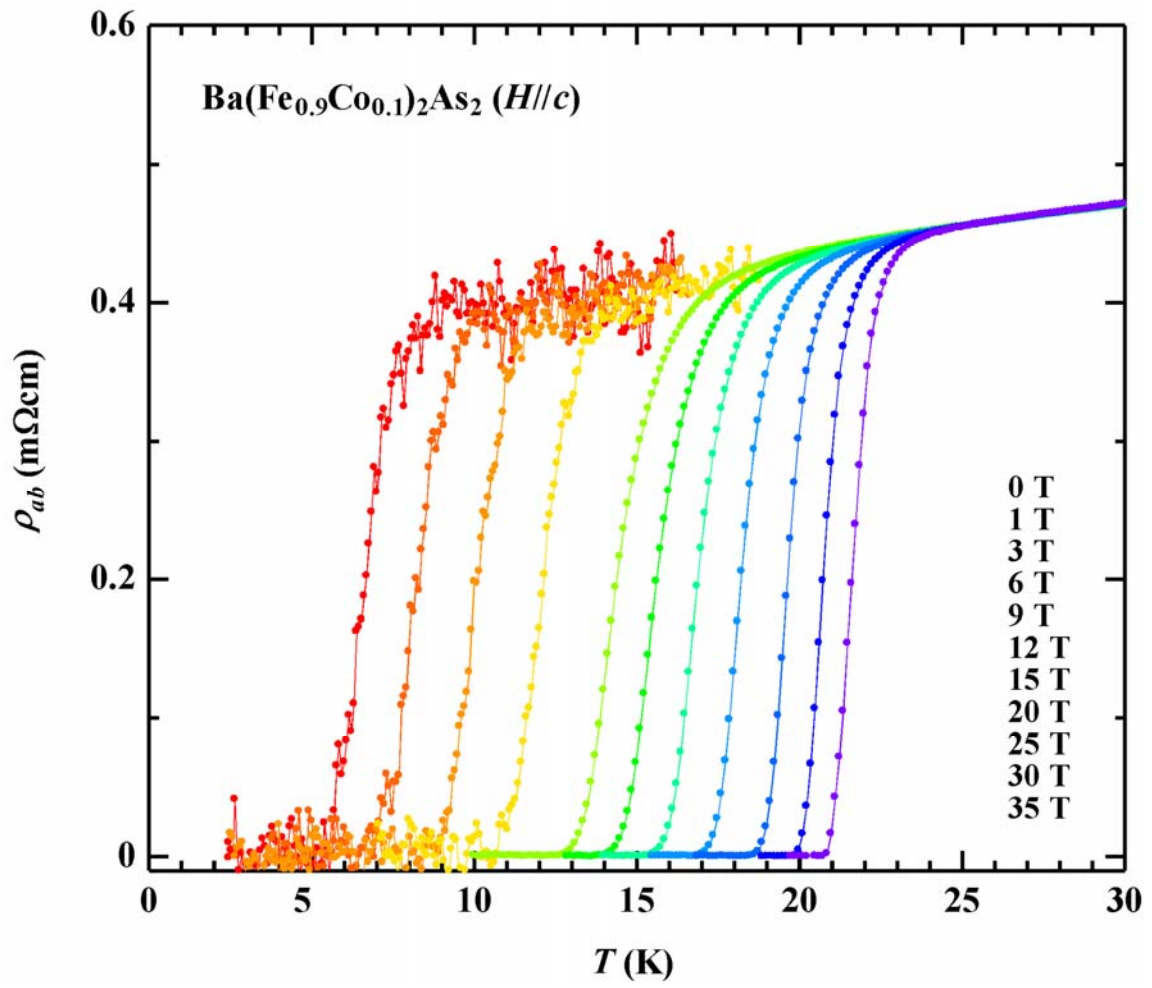
Yamamoto et al.

Figure 3



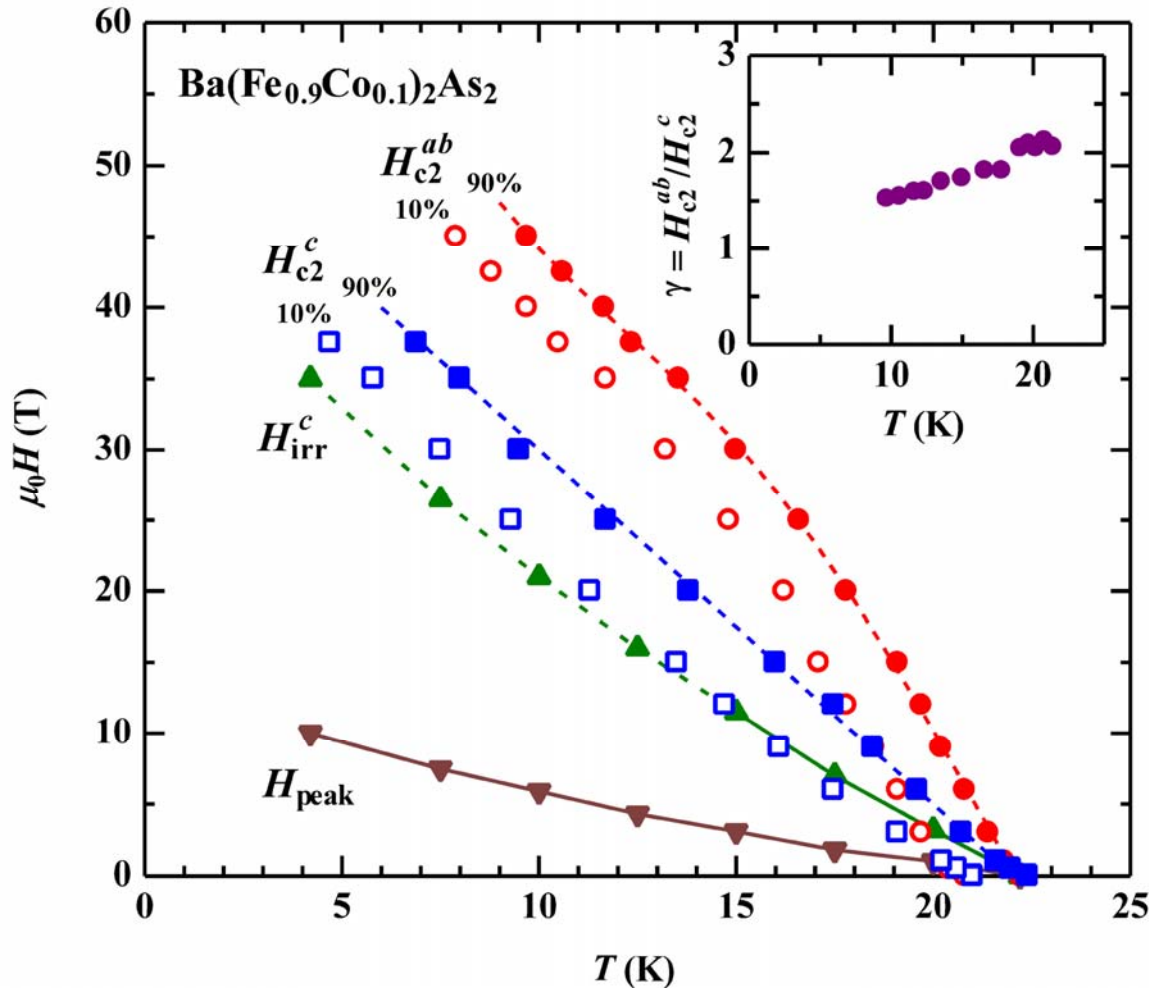
Yamamoto et al.

Figure 4



Yamamoto et al.

Figure 5



Yamamoto et al.